FULL PAPER

All-Solution-Processed Random Si Nanopyramids for Excellent Light Trapping in Ultrathin Solar Cells

Sihua Zhong, Wenjie Wang, Yufeng Zhuang, Zengguang Huang, and Wenzhong Shen*

Si nanopyramids have been suggested as one of the most promising Si nanostructures to realize high-efficient ultrathin solar cells or photodetectors due to their low surface area enhancement and outstanding ability to enhance light absorption. However, the present techniques to fabricate Si nanopyramids are either complex or expensive. In parallel, disordered nanostructures are believed to be extremely effective to realize broadband light trapping for solar cells. Here, a simple and cost-effective method is presented to form random Si nanopyramids based on an all-solution process, the mechanism behind which is the successful transfer of the generation site of bubbles from Si surface to the introduced Ag nanoparticles so that OH⁻ can react with the entire Si surface to naturally form random and dense Si nucleus. For optical performance, it is experimentally demonstrated that the random Si nanopyramid textured ultrathin crystalline Si (c-Si) can achieve light trapping approaching the Lambertian limit. Importantly, it is revealed, by numerical calculations, that random Si nanopyramids outperform periodic ones on broadband light absorption due to more excited optical resonance modes. The finding provides a new opportunity to improve the performance of ultrathin c-Si solar cells with a simpler process and lower cost.

1. Introduction

Realizing excellent light trapping is the crucial point for ultrathin solar cells to maintain the comparable photon absorption and thus the efficiency with their bulk counterparts. Among various light trapping strategies based on Si nanostructures,[1–3] Si nanopyramids (including upright and inverted) have particularly attracted research interests. On the one hand, excellent light trapping effect of Si nanopyramids has been demonstrated in both experiment and simulation.[4–6] On the other hand, their surface area is only 1.7-fold the planar surface, far lower than that of other Si nanostructures such as nanowires and nanoholes, hence resulting in lower surface recombination.[7,8]

In general, Si pyramids are formed through anisotropic etching in alkaline solution and the typical sizes are 5–10 μm. To reduce the pyramid size and thickness loss, a thin dielectric mask such as SiO_2 or SiN_x can be deposited on Si surface and then the Si wafer is directly etched in alkaline solution without lithography process.[9,10] The produced Si pyramids have a size of 2–4 μm. Free of the mask, it is reported that small Si pyramids with sizes around 2 μm can be produced through using a special surface additive and controlling its ratio.[11] And Li et al.[12] have fabricated Si pyramids with sizes of 1–3 μm by replacing NaOH or KOH solution with NaClO, which is an alkaline and strong oxidizing reagent. Amazingly, pyramid structure can be also formed in acid solution ($HF/H_2O_2/H_2O$) by the aid of Cu nanoparticles, but the pyramidal size is still larger than 2 μm with etching depth in the range of 1–5 μm.[13] Though the above methods are simple, they are hard to generate uniform Si pyramids with nanoscale sizes.

The techniques to form Si nanopyramids have thus become a focus of concern. Nanoimprint lithography (NIL) method is one of the most popular methods for Si nanopyramid formation.[5,14,15] And for most NIL process, first, a dielectric layer (SiO_2 or SiN_x) is grown on Si surface as etching mask, followed by the deposition of photoresist layer and NIL to define the etching pattern, and then reactive ion etching and HF solution are used to remove the residual photoresist and the dielectric layer in the opening window, and finally anisotropic etching is carried out to form Si nanopyramids. Another technique employing focus ion beam has been introduced by Koh et al.[16] The Si wafer surface is selectively irradiated by focus ion beam, and the Si nanopyramids are formed by utilizing the retarded etching rate of the ion beam exposed Si in $N_2H_4H_2O$ solution. Mavrokefalos et al.[7] and Branham et al.[6] have fabricated inverted nanopyramids based on interference lithography and wet Si etching. This technique needs to form a SiO_2 and photoresist layers on the wafer surface first, and then uses interference lithography method to define etching pattern, followed by wet etching in alkaline solution. As can be seen, most of the fabrication techniques of Si nanopyramid structures are either complicated or expensive, and the reported Si nanopyramids are periodic.

Dr. S. Zhong, W. Wang, Y. Zhuang, Dr. Z. Huang,
Prof. W. Shen
Institute of Solar Energy
Key Laboratory of Artificial Structures and Quantum
Control (Ministry of Education)
Department of Physics and Astronomy
Shanghai Jiao Tong University
Shanghai 200240, P. R. China
E-mail: wzshen@sjtu.edu.cn
Prof. W. Shen
Collaborative Innovation Center of Advanced Microstructures
Nanjing 210093, P. R. China

www.MaterialsViews.com

ADVANCED
FUNCTIONAL
MATERIALS
www.afm-journal.de

FULL PAPER

However, periodic nanostructures with mirror symmetry such as regular Si nanopyramids will lead to the degeneracy of the optical resonance modes that contributes to the increased light absorption.[4,17] In contrast, recent literatures argue that random nanostructures are more helpful to achieve broadband enhancement of light absorption.[18–21] Sturmberg et al.[20] have discerned that random Si nanowires with various radii perform better than the ones with identical radius on light absorption because of more excited resonance modes. Besides the size of nanostructures, it is also experimentally demonstrated that increasing disorder in position is more beneficial for nanophotonics to achieve broadband light trapping as compared to the periodic counterpart.[21]

Here, we propose a simple, cost-effective, and mass-production compatible method to fabricate random Si nanopyramids based on a layer of Ag nanoparticles and wet Si etching. It does not involve the deposition of dielectric layers, photoresist, or ion etching process, and is an all-solution processing technique. The successful fabrication of the Si nanopyramids lies in the transfer of the resultant electrons in the etching process from Si to Ag nanoparticles, resulting in the formation of bubbles on Ag surface rather than on Si surface so that OH^- can react with the whole Si surface to naturally form random and dense Si pyramid nucleus. Utilizing the random Si nanopyramids as surface texture, near-Lambertian light trapping effect[22,23] is achieved in ultrathin crystalline Si (c-Si) with thickness of 30 μm in experiment, showing a significant enhancement of light absorption as compared with planar surface. We have also carried out simulations to further explore the advantages of our fabricated Si nanopyramids on 3 μm ultrathin c-Si substrates and reveal that random Si nanopyramids can excite more optical resonance modes than periodic ones to realize outstanding broadband light absorption.

2. Formation of Random Si Nanopyramids

Figure 1 shows scanning electron microscopy (SEM) images, digital photograph, as well as reflectance of the silicon surface treated with different texturing methods. Figure 1a is the top view of random Si micropyramids formed by the conventional texturing method for single-crystalline Si solar cells.[24] Although most of the Si pyramids have a lateral size of about 5 μm, one can still see that the pyramid sizes differ noticeably in the range of 1–10 μm. Note that for the conventional texturing method, solution temperature needs to be maintained at about 80 °C and etching time 30–50 min. When decreasing the solution temperature to 65 °C and the etching time to 20 min, only several pyramids with sizes of 1–2 μm are sparsely formed on the Si wafer surface (see Figure 1b), demonstrating that the surface texture is ineffective. However, if the Si wafer is decorated with a thin layer of Ag nanoparticles on the surface by being immersed in $AgNO_3$/HF solution first, and then etched in NaOH solution for 20 min at a temperature of 65 °C, it is amazing that its surface morphology is completely different from the two samples described above, as shown in Figure 1c,d (zoomed-in SEM image). The Si pyramids are densely and randomly distributed on the wafer surface (some are overlapped),

exhibiting a perfect surface texture. Their lateral sizes mainly range from 300 to 600 nm.

To evaluate the optical performance of the nanopyramids, the reflectance (R) and absorptance (A_b) spectra of different surface condition are compared in Figure 1e. Compared to the micropyramid counterpart, the nanopyramid textured wafer has a little higher reflectance over the whole wavelength range from 400 to 1100 nm due to its much smoother surface. But the gap between these two reflectance spectra is reduced when the Si surfaces are coated by SiN_x antireflection layer. Also, from the view of fabrication process, the nanotexture has much less material loss (the thickness loss via the proposed nanotexture method can be controlled to 0.8–1.5 μm per side, while that of the micropyramid texture reaches around 5 μm per side), which is highly significant for the application in ultrathin c-Si solar cells. For example, the nanopyramid textured c-Si film with a thickness of 73 μm possesses a superior A_b in the long wavelength than the micropyramid textured one despite its higher reflectance, as shown in Figure 1e. This is mainly ascribed to more absorber layer kept. We believe that the thinner the c-Si film, the advantage of the nanopyramid texture is more prominent. Micropyramid texture is not applicable for the c-Si film with a thickness smaller than 10 μm.[6,7]

Our proposed new technique for random Si nanopyramid preparation is an all-solution-processed method and thus does not involve any electron or ion etching, or dielectric masking layers as are required in focus ion beam etching, interference lithography, and nanoimprint lithography techniques. Although noble metal is contained, the concentration of $AgNO_3$ is ultralow (7.8×10^{-3} M). Therefore, the fabrication method is very simple and cost-effective. It is worth mentioning that the nanopyramid texturing method can be applied to quasi 156 mm × 156 mm wafers. As shown in Figure 1f, different positions of the Si wafer have almost the identical reflectance over the whole wavelength, demonstrating the uniform surface texture.

3. Formation Mechanism of the Si Nanopyramids

Figure 2a,b presents the top-view and cross-sectional SEM images of the textured Si surface without the removal of Ag nanoparticles after being etched in alkaline solution for 20 min under the temperature of 65 °C. Distinctly, the Ag nanoparticles are randomly distributed on the top, bottom, and slope facet of the Si pyramids, unlike the case that Ag nanoparticles are embedded at the bottom of Si nanopores in $HF-H_2O_2$/HNO_3-H_2O etching system because of their catalytic role.[25,26] Therefore, in our alkaline etching system, the Ag nanoparticles are not a catalytic agent, or at least they do not locally accelerate the etching. However, the existence of Ag nanoparticles significantly affects the anisotropic etching process of Si. On the one hand, Ag nanoparticles enhance the density of the pyramid nucleus. With Ag nanoparticles deposited on the surface, highly dense Si hillocks, which are the nucleus of Si pyramids, are formed after just being etched for 3 min under the solution temperature of 65 °C, as illustrated in Figure 2c, while the Si wafer without Ag nanoparticles has much sparse and smaller hillocks on the surface under the same etching condition, as shown in Figure 2d.
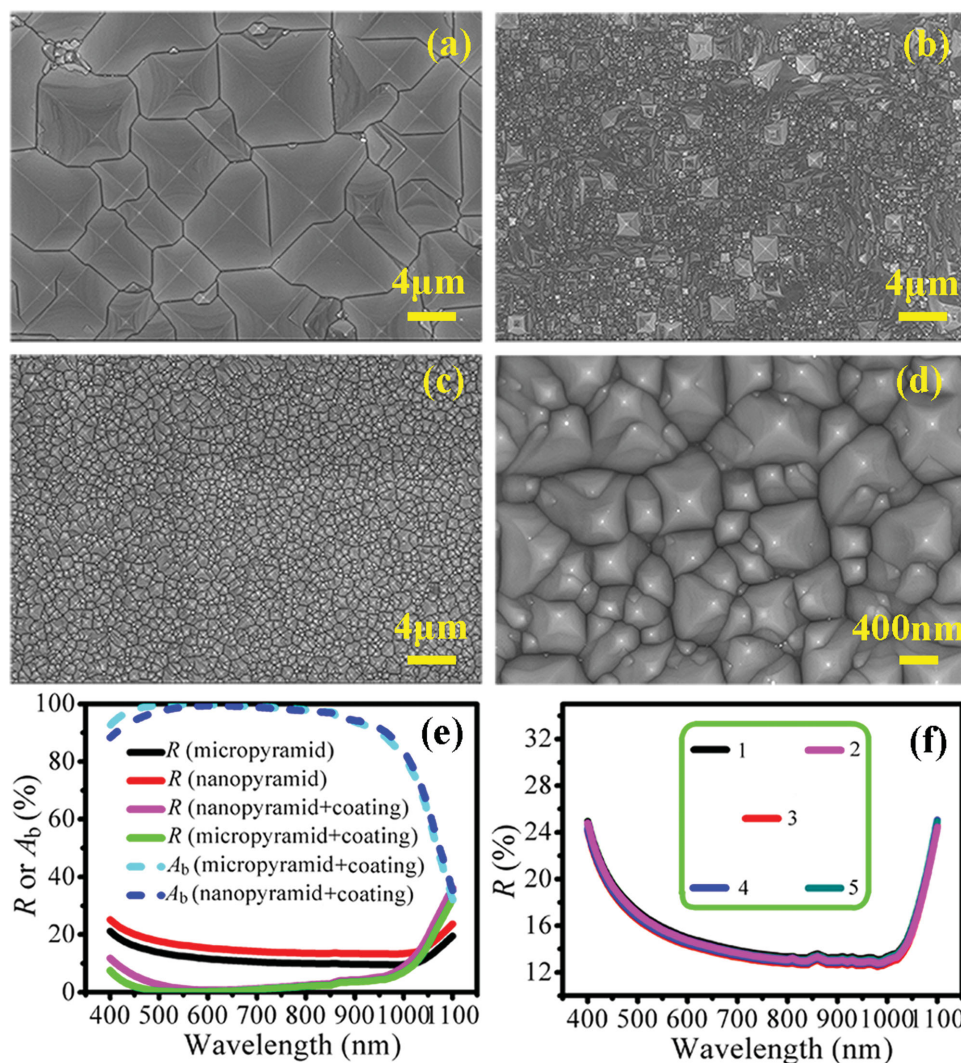
FULL PAPER

Figure 1. Top-view SEM images of the textured Si surface with different texturing condition. a) The conventional micropyramidal texture formed in alkaline solution with temperature of 80 °C and etching time of 40 min. b) The surface textured in alkaline solution with temperature of 65 °C and etching time of 20 min. c) The nanopyramids formed by immersing in AgNO$_3$/HF solution for 10 s to form a thin layer of Ag nanoparticles, followed by etching in the alkaline solution with temperature of 65 °C and etching time of 20 min. d) Zoomed-in SEM image of (c). e) Comparisons of R and A_b of the micropyramid and nanopyramid textured wafers with and without SiN$_x$ coating. f) Reflectance spectra of the different positions on a large-size nanopyramid textured Si wafer surface (quasi 156 mm × 156 mm). The numbers schematically show the measured positions.

On the other hand, we find that ultrasmall bubbles are generated and escape away rapidly from the Si wafer decorated with Ag nanoparticles through observing the etching process. In contrast to this, for the Si wafer without Ag nanoparticles, relatively larger bubbles in the etching process are produced and then escape away more slowly. Moreover, some bubbles adhere on the Si surface, which is obviously presented in Figure 2e. From the observation, we speculate that the etching rate is faster for the Si wafer coated with Ag nanoparticles. To confirm this, we have monitored the mass loss to calculate the effective thickness loss per side (ΔW) and thus extract the etching rate. The ΔW is calculated by the following equation

$$\Delta W = \frac{m_{\text{before}} - m_{\text{after}}}{m_{\text{before}}} \times \frac{W}{2} \qquad (1)$$

where m_{before} and m_{after} represent the mass of wafer before and after etching, respectively, and W is the wafer thickness before etching (the thickness of polished wafer is around 180 μm). Figure 2f explicitly shows that the ΔW of the Si wafer with Ag nanoparticles is higher compared to the one without Ag nanoparticles no matter the etching time short or long. And through linearly fitting the ΔW versus etching time, the etching rate of Ag nanoparticles decorated Si wafer is calculated to be 0.075 μm min^{-1}, indeed higher than that of the naked Si wafer (0.060 μm min^{-1}).

To get insight into the phenomena above and understand the role of Ag nanoparticles in the study, it is necessary to know the etching mechanism of Si in alkaline solution. For example, for a (100) surface of Si, OH$^-$ ions attack the Si surface and two ions are bound to per surface atom through dangling bonds with injecting two electrons into the conduction band, namely[27]
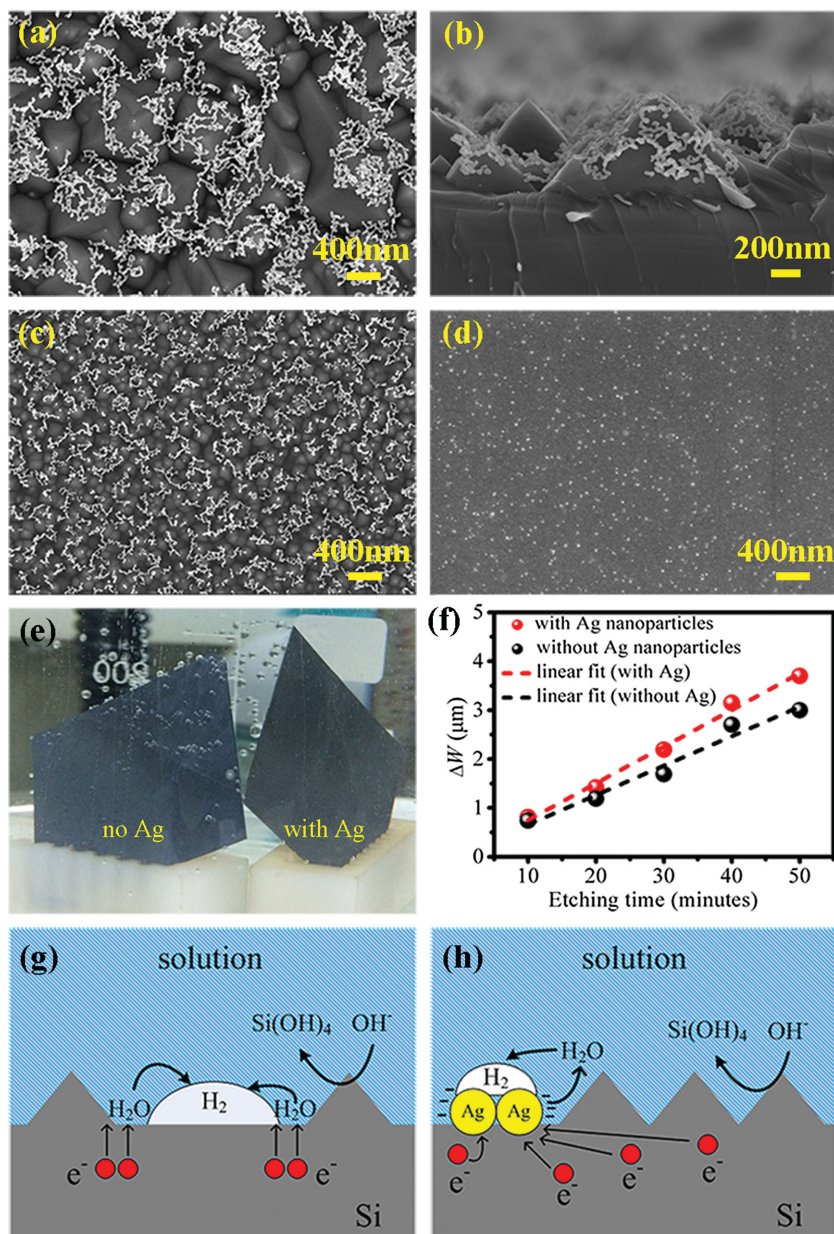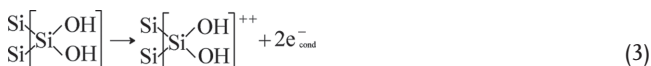
Figure 2. a) Top-view and b) cross-sectional SEM of the distribution of Ag nanoparticles on the Si nanopyramid textured surface. SEM image of the surface morphology of the Si etched in a temperature of 65 °C for 3 min c) with and d) without the deposition of Ag nanoparticles, which characterize the pyramid nucleus. e) Comparison of the etching process of the Si with and without the deposition of Ag nanoparticles on the surface. The bubbles are obviously different. f) Effective thickness loss (ΔW) of the Si wafer with and without Ag nanoparticles as a function of etching time. Schematic diagrams of the etching mechanism of Si wafer in alkaline solution g) without and h) with the deposition of Ag nanoparticles on the surface.

$$\underset{Si}{\overset{Si}{>}}Si + 2\,OH^- \longrightarrow \underset{Si}{\overset{Si}{>}}Si\underset{OH}{\overset{OH}{<}} + 2e^-_{cond} \qquad (2)$$

In the next step, the Si(OH)$_2$ groups transform into a positively charged silicon hydroxide complex by thermally exciting the electrons into the conduction band

$$\underset{Si}{\overset{Si}{\Big[}}Si\underset{OH}{\overset{OH}{<}}\Big] \longrightarrow \underset{Si}{\overset{Si}{\Big[}}Si\underset{OH}{\overset{OH}{<}}\Big]^{++} + 2e^-_{cond} \qquad (3)$$

Then the positively charged silicon-hydroxide further reacts with the OH$^-$ ions producing soluble silicic acid

$$\underset{Si}{\overset{Si}{\Big[}}Si\underset{OH}{\overset{OH}{<}}\Big]^{++} + 2\,OH^- \longrightarrow Si(OH)_4 + Si_{solid} \qquad (4)$$

At the same time, the excited electrons are transferred to water molecules near the Si surface, resulting in the following reduction reaction

$$4H_2O + 4e^- \rightarrow 4H_2O^- \qquad (5)$$

$$4H_2O^- \rightarrow 4OH^- + 4H \rightarrow 4OH^- + 2H_2 \qquad (6)$$
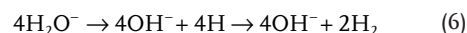
As shown in the schematic diagram (Figure 2g), for the Si wafer without Ag nanoparticles, OH$^-$ ions attack the Si surface and react with Si atoms to form Si(OH)$_4$. Meanwhile, the generated electrons are directly injected to the water molecules located near the Si surface, producing hydrogen atoms. Then the hydrogen atoms evolve into H$_2$ molecules and adhere to Si surface, accumulating to form H$_2$ bubbles. The bubbles have a mask effect so that the Si beneath them is prevented from reacting with OH$^-$ ions, hence leading to the lower etching rate and the sparse Si pyramids. (Note that for conventional micropyramidal texture process, the solution temperature is 80 °C, so the etching process is significantly accelerated. Furthermore, the etching time is longer and the anisotropic factor is increased too. Therefore, more Si surface is etched and compact micropyramids can be formed.) For the case with Ag nanoparticles (see Figure 2h), instead of being injected into water molecules from Si directly, we believe that the generated electrons are extracted by the Ag nanoparticles first due to the higher electronegativity of Ag than Si[25,28] and thereby make the Ag negatively charged. Then the accumulated electrons are transferred to the water molecules located near the Ag nanoparticles, which produces H$_2$ bubbles adhering on the Ag surface with much smaller size. Without large bubbles on the Si surface and that the Ag particles are nanoscale size, OH$^-$ ions can react with nearly the whole Si surface to result in compact pyramid nucleation, thereby the dense Si nanopyramids. Also, the etching rate is greatly increased. However, it should be pointed out here that the Ag nanoparticles do not act as a catalytic agent that accelerates the etching locally but mainly collect electrons from the conduction band, which is different from the case in acid solution.[25,26,29] Moreover, we want to clarify that a wetting agent such as isopropyl alcohol (IPA) is needed

ADVANCED
FUNCTIONAL
MATERIALS

www.afm-journal.de

Materials
Views

www.MaterialsViews.com

to obtain sufficient wettability for the Si surface by reducing the Si/electrolyte interfacial energy.[24] If there is no IPA, the wettability is not good enough. Thus the bubbles formed on the Ag nanoparticles will extend to Si surface and combine the adjacent bubbles to form larger ones. Eventually, large bubbles will strip off the Ag nanoparticles and thus lead to the etching process similar to the case without depositing Ag nanoparticles. Therefore, the success of forming the nanoscale Si pyramids is attributed to the comprehensive effect of Ag nanoparticles and the IPA. Considering the fact that IPA is also needed to obtain good wettability in the micropyramidal texturing technique, this study will mainly stress the impact of Ag nanoparticles.

4. Influence of Solution Temperature and Etching Time on Morphology

In order to get more knowledge of the novel method, we have investigated the influence of solution temperature on the surface morphology, solar spectrum averaged reflectance (R_{ave}), as well as ΔW with a fixed etching time of 25 min. When the solution temperature is lower than 45 °C, the wafer surface looks almost the same as that before etching because the etching rate is too slow and thereby only ultrasmall hillocks are formed (whose SEM is not shown here). However, when the solution temperature is higher than 55 °C, the wafer surface looks dark gray color, suggesting effective surface texture. **Figure 3** shows the SEM images of the Si surface etched under the solution temperatures of 55, 65, 75, and 85 °C as well as their statistical size distribution. It can be seen that all the surfaces are compactly covered with Si pyramids of different sizes. The Si pyramids fabricated under the temperature of 55 °C have sizes distributed from 100 to 1100 nm with a mean value of 443 nm. The standard deviation (SD), which is a parameter to quantify the dispersion of a set of data, of the size of the Si nanopyramids is 206 nm, indicating that the pyramid sizes are mainly distributed from 250 to 650 nm. With regard to the ones fabricated under the temperature of 65 °C, the sizes are distributed from 100 to 1200 nm but most of them are concentrated in 250–670 nm because their mean value is 467 nm and SD is 210 nm, showing an extremely slight increase of size as compared to that of the 55 °C case. However, when increasing the solution temperature to 75 °C, the mean value and SD of the size of the Si pyramids are also increased to be 579 and 329 nm, respectively. This means that the sizes are mainly concentrated
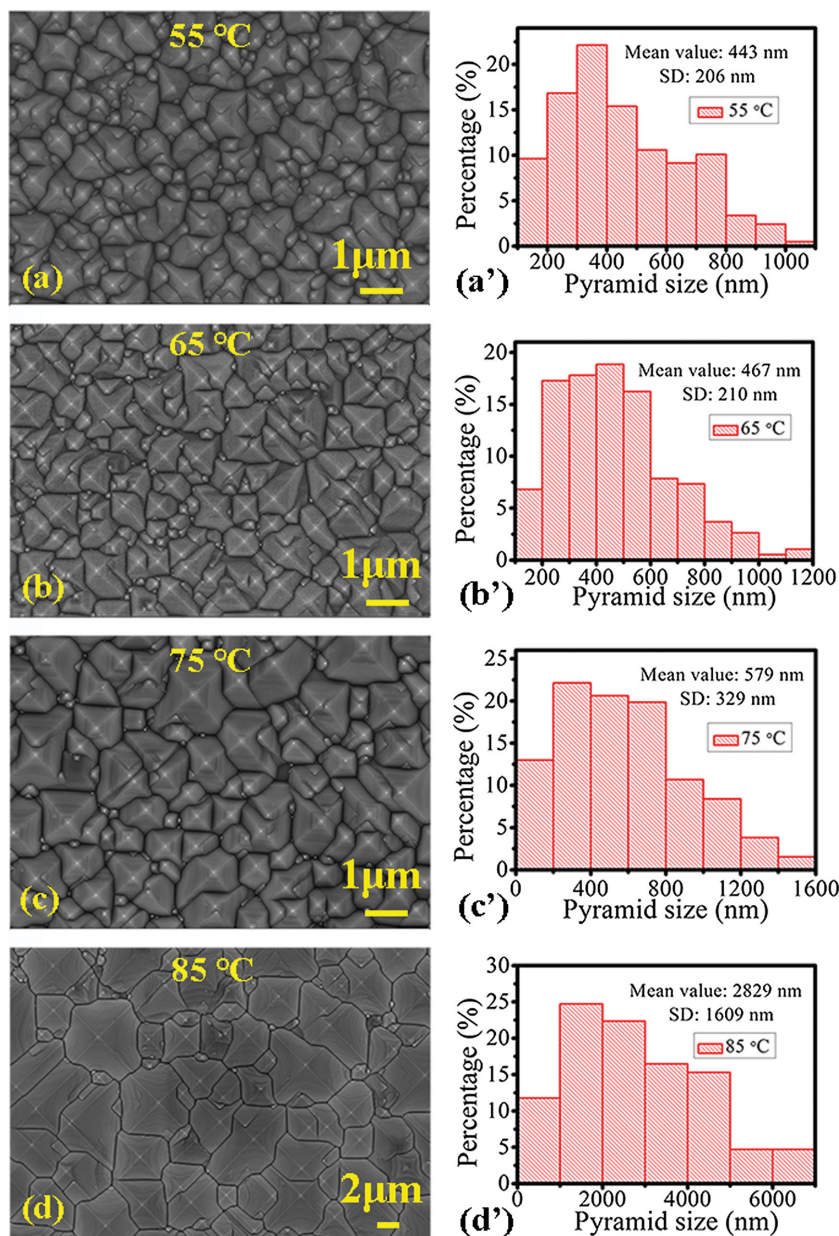

Figure 3. SEM images of the surface morphologies of the Si wafers etched under the solution temperatures of a) 55 °C, b) 65 °C, c) 75 °C, and d) 85 °C. The corresponding statistical data of the pyramid size are shown in a'), (b'), c'), and d'), respectively.

in 250–900 nm. The increase of size may be attributed to the increased difference of etching rate between the (100) and (111) crystallography plane as solution temperature increasing.[30] When the solution temperature is increased to 85 °C, the fabricated Si pyramids have sizes distributed from several hundred nanometers to about 7 μm with a mean value of 2829 nm and SD of 1609 nm, presenting a dramatic increase of the pyramid size. In this case, the fabricated Si pyramids are similar to the ones formed by the conventional Si anisotropic etching method. Besides the increased difference of etching rate between the (100) and (111) crystallography plane, the failure in preparing Si nanopyramids under the temperature is also
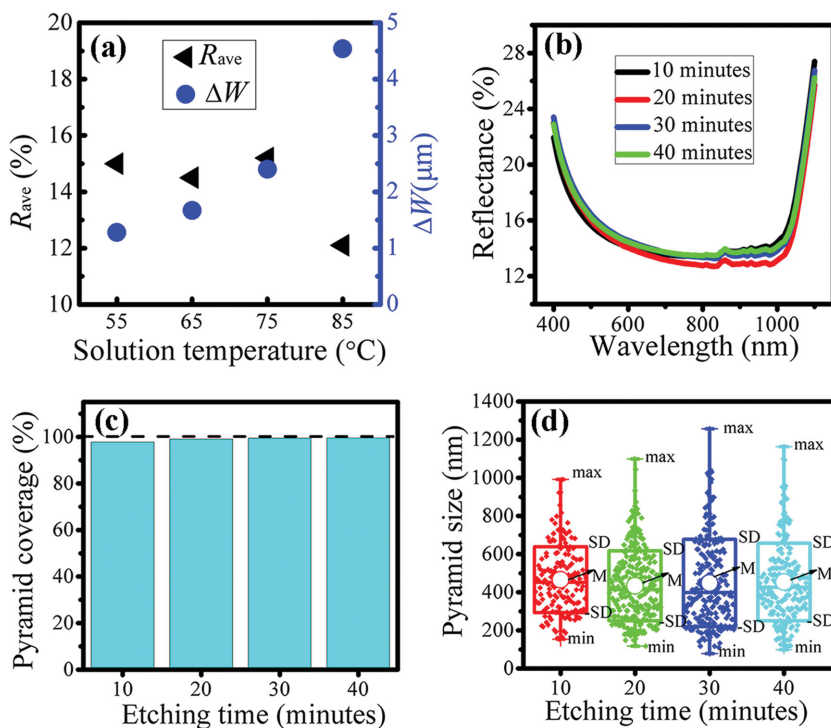
www.MaterialsViews.com

ADVANCED
FUNCTIONAL
MATERIALS
www.afm-journal.de

FULL PAPER

Figure 4. a) Variation of R_{ave} and ΔW with solution temperature. b) Reflectance spectra, c) pyramid coverage, and d) pyramid size distribution of the Si wafers etched under the temperature of 65 °C varying with etching time from 10 to 40 min. In the figure, max and min represent the maximum and minimum data, respectively. M is the mean value of the data.

attributed to that a large number of electrons are fast generated from the intense reaction, resulting in the injection of electrons into the water molecules not only from Ag nanoparticles but also from Si surface directly, thus similar to the conventional etching process.

On the aspect of optical performance, **Figure 4**a shows that the R_{ave}s of the Si wafers are almost equivalent (14.5%–15.2%) when the solution temperature is between 55 and 75 °C, which is ascribed to their similar surface morphology as discussed above. When the temperature further increases to 85 °C, the R_{ave} dramatically reduces to about 12%. However, ΔW increases rapidly with solution temperature and reaches 4.5 μm at the temperature of 85 °C. And as discussed in Section 2, the reflectance gap between these wafers will diminish after the deposition of antireflection coating. Therefore, based on the comprehensive consideration of surface micromorphology, optical performance, and material loss, from the view of application in ultrathin c-Si solar cells, the etching temperature should be selected as 55–65 °C, under which the formed Si pyramids possess stable surface morphology (due to its insensitive to the temperature in the range), good antireflection property, and low thickness loss.

We have also investigated the effect of etching time on surface micromorphology, reflectance spectrum, and ΔW under the fixed solution temperature of 65 °C. From Figure 4b, it can be seen that the reflectance curves of the wafers with different etching time are highly closed, indicating the insensitive of reflectance on etching time. This can be also understood from their surface micromorphologies. All the

surface coverage of Si pyramids fabricated with different etching duration approaches 100% (Figure 4c), even the etching time as short as 10 min. Moreover, the sizes of the Si pyramids are insensitive to the etching time. The mean values and SD of the Si pyramids fabricated with etching time from 10 to 40 min are about 450 and 200 nm, respectively, indicating that most of the pyramid sizes are distributed from 250 to 650 nm, as presented by the data in the boxes in Figure 4d. Although the Si pyramids have similar size distributions, the ΔW increases obviously with the etching time, as presented in Figure 2f. Hence, shorter etching time (10–20 min) is preferred to control the thickness loss without losing optical performance.

5. Light Absorption in Ultrathin c-Si

One of the most important applications of the Si nanopyramids is to provide light trapping in ultrathin c-Si solar cells. In general, the absorber thickness of ultrathin c-Si cells is only a few tens of micrometers (<40 μm) or even several micrometers, whereas the formation of conventional micropyramids needs a material thickness loss of several micrometers, making it unsuitable as the light trapping layer due to the concerns of retaining the absorber thickness. Instead, Si nanostructure textures can not only effectively reduce surface reflection but also induce little optical absorber loss. However, the present Si nanostructures either lead to high carrier recombination or need a sophisticated fabrication process. Here, we have successfully fabricated random Si nanopyramids, which have low surface area enhancement, on thin film c-Si layer as surface texture through the all-solution-processed technique. Then both the front and rear surfaces are coated by SiN_x layer together with an Ag film deposited on the rear side as the back reflector. **Figure 5** shows that the Si nanopyramids are densely and randomly distributed on the ultrathin c-Si surface with most lateral sizes of 250–650 nm. The height of the Si nanopyramids is only about 250–350 nm, far lower than the 30-μm-thick ultrathin c-Si layer, ensuring the minimal loss of the absorber volume. SiN_x layers are conformally coated on the nanopyramid surfaces with a layer thickness of 75 nm at the front side and 100 nm at the back side. Ag film is also conformally deposited on the back SiN_x layer with a thickness of about 150 nm by electron beam evaporation technique.

Figure 6a displays absorptance of the random Si nanopyramid textured and the planar ultrathin c-Si as a function of wavelength. The absorptance spectrum of the same ultrathin c-Si in the Lambertian light trapping limit is also calculated and presented as reference. With assumption that the external reflectance of front surface is 0, internal reflectance of rear
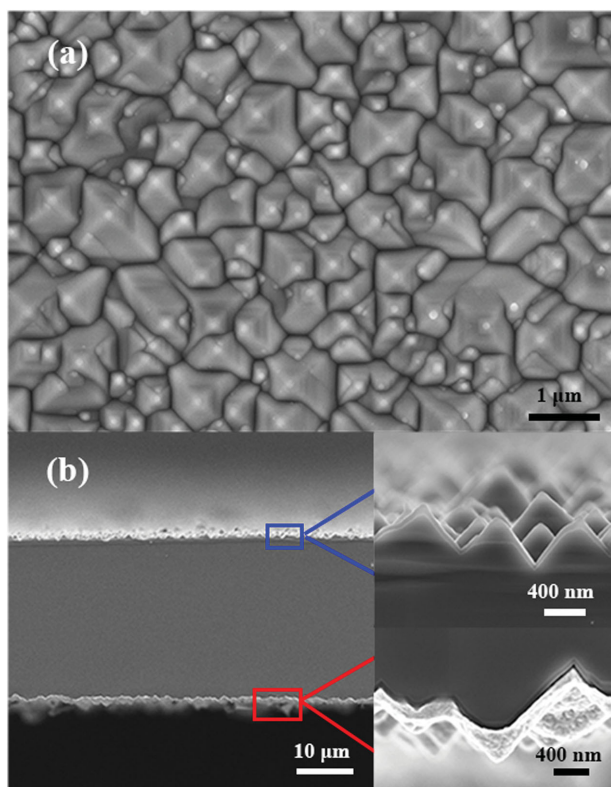
ADVANCED
FUNCTIONAL
MATERIALS
www.afm-journal.de

Materials
Views
www.MaterialsViews.com

FULL PAPER

Figure 5. a) Top-view SEM image and b) cross-sectional SEM image of the ultrathin c-Si structure. The right bottom images are close-ups of the blue and red boxed regions.

surface is 1, and considering the weak absorption condition, then the Lambertian limit is expressed as[22,23]

$$A_b = \frac{4n^2 \alpha W}{1 + 4n^2 \alpha W} \qquad (7)$$

where W is device thickness and n and α represent refractive index and absorption coefficient, respectively. In this case, it is also often called Yablonovitch limit.[23] It can be seen that the optical absorption of the planar thin film c-Si layer depends strongly on photon wavelength, approaching 100% absorptance only in the destructive interference region (the thickness of the SiN$_x$ layer on the planar ultrathin c-Si is about 83 nm), while decreasing rapidly outside the region. By contrast, the nanopyramid textured ultrathin c-Si shows high optical absorptance over a wide wavelength range, closely approaching the Lambertian limit, demonstrating the extraordinary light trapping effect of our fabricated Si nanopyramids. Through the absorptance spectra, we calculated the potential short circuit current density (J_{SC}) of our experimental ultrathin c-Si samples based on the following equation

$$J_{SC} = \int_{AM1.5} q \cdot A_b(\lambda) \cdot IQE(\lambda) d\lambda \qquad (8)$$

where q is elemental charge, $A_b(\lambda)$ is the absorptance spectrum, and IQE(λ) is the internal quantum efficiency spectrum (here, it is assumed to be 100% in the whole wavelength). Figure 6b presents the calculated J_{SC} of the planar, random nanopyramid textured, and Lambertian absorbed ultrathin c-Si under AM1.5 spectrum. Remarkably, the J_{SC} of the nanopyramid textured ultrathin c-Si sample is much higher than that of the planar one and is close to the Lambertian limit, reaching as high as 38.6 mA cm^{-2} on an ultrathin c-Si with only 30 μm in thickness. Though the absorption in Ag film is not considered in the calculation above, we find that it can be neglected compared to the absorption in the c-Si layer based on the simulation of a similar ultrathin c-Si solar cell with periodic nanopyramid texture by finite-difference time-domain (FDTD) calculation (see Figure 6a), which also agrees with the result of Mavrokefalos et al.[7] Such a result is attributed to our rational design of the rear SiN$_x$ layer. We have carefully investigated the dependence of the Ag absorption on the thickness of the rear SiN$_x$ layer by FDTD simulation, as presented in Figure 6c. When the thickness of the rear SiN$_x$ layer is 0 nm, namely, no SiN$_x$ layer, the Ag film clearly has a high optical absorption in the long wavelength range. Nevertheless, when the thickness of the SiN$_x$ layer reaches 10 nm, the optical absorption in the Ag layer is dramatically reduced. It will be further decreased with increasing SiN$_x$ layer thickness to the lowest absorptance of about 3% for SiN$_x$ thickness larger than 30 nm, which benefits from the reduced coupling of evanescent wave into the Ag film and thus the decreased excited surface plasmon resonance.[31] Therefore,
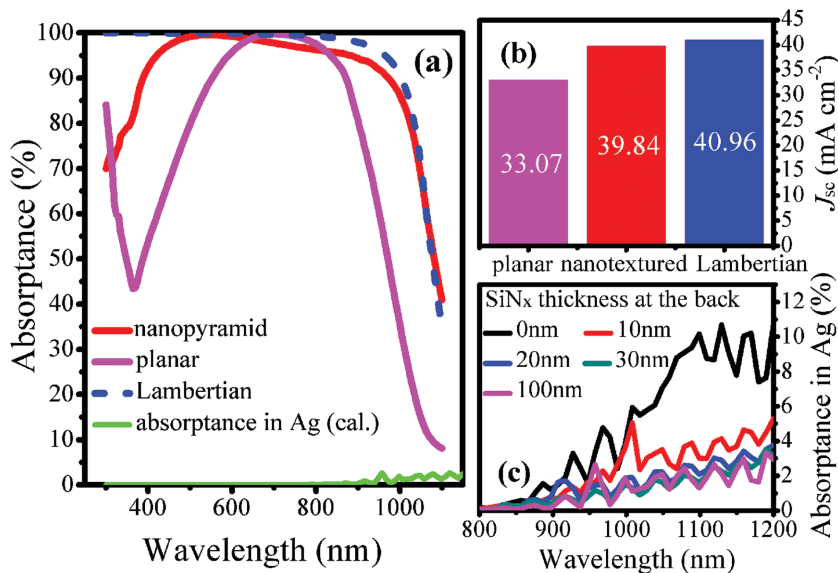

Figure 6. a) Comparison of the experimental absorptance spectra of the nanopyramid textured and planar ultrathin c-Si layer with a thickness of 30 μm. The absorptance spectrum in the Lambertian limit is also presented as a reference. The absorptance in the Ag film is calculated by the FDTD method. b) Calculated J_{SC} of the ultrathin c-Si with planar surface, our silicon nanopyramid textured surface, and Lambertian surface based on the absorptance spectra in (a). c) Absorptance in the Ag film varying with the thickness of the rear SiN$_x$ layer by FDTD calculation.

Materials
Views

www.MaterialsViews.com

ADVANCED
FUNCTIONAL
MATERIALS
www.afm-journal.de

FULL PAPER

the optical absorption in the Ag layer can be neglected when the SiN$_x$ layer thickness is 100 nm in our study. However, it should be pointed out that the SiN$_x$ layer needs to be locally opened by laser to make the Ag layer locally contact the Si for collecting current in a real solar cell. Therefore, though the optical advantage of the SiN$_x$/Ag bilayer is basically retained, the light absorption in a real cell should be smaller than the result claimed due to the large parasitic absorption in the local Ag/Si contacts.

6. Advantage and Mechanism of Random Si Nanopyramids on Light Trapping

To further understand the advantage of our fabricated Si nanopyramids and the mechanism of excellent light trapping effect behind them, we have simulated the light absorption in 3-µm-thick c-Si thin film with planar, periodic, and random Si nanopyramid textured surface, respectively. In the case of random Si nanopyramids, both the size and position are disordered (sizes are randomly distributed from 300 to 700 nm and some pyramids are overlapped), similar to our experimentally fabricated pyramids. In the periodic case, the size of the pyramid is 500 nm, approaching the average size of the experimental ones. All the ultrathin c-Si films are single-side textured instead of double-side textured that is adopted in the experiment. As shown in **Figure 7**, double-side-textured c-Si film is less efficient
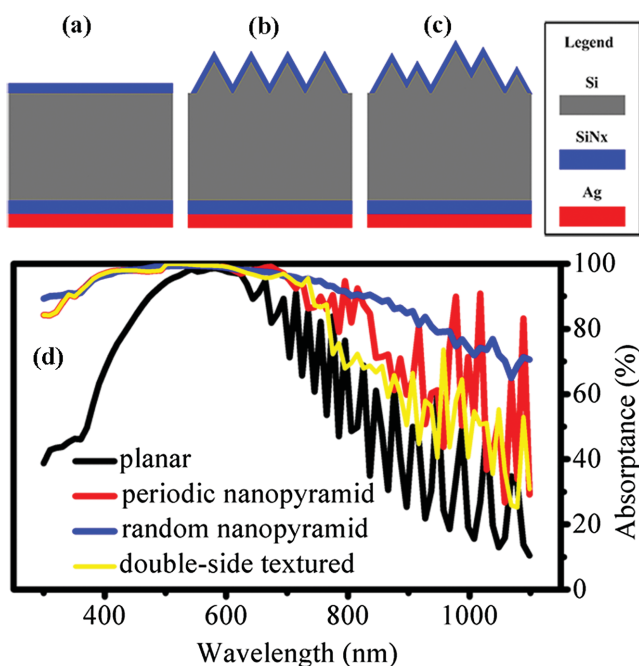

Figure 7. Structural diagrams of the ultrathin c-Si with a) planar, b) periodic Si nanopyramid, and c) random Si nanopyramid textured surface in the simulation by FDTD. The thickness of the ultrathin c-Si film is 3 µm and all front surfaces are covered by SiN$_x$ layer with 75 nm in thickness. The back sides are coated with both SiN$_x$ layer (inner coating) and Ag layer (outer coating). d) Calculated light absorptance in the ultrathin c-Si with different surface textures as a function of wavelength ranging from 300 to 1100 nm. Absorption of double-side periodic Si nanopyramid textured device is also presented for comparison.

in increasing light absorption in Si due to the higher absorption in the back Ag reflector. One of the possible reasons is the increased Ag interface. Fortunately, real ultrathin c-Si solar cells are generally single-side textured.[1,6] Therefore, it is more meaningful to demonstrate the benefit of the random Si nanopyramids by single-side texture design. The detailed structure configurations are illustrated in Figure 7a–c. As can be seen in Figure 7d, the planar ultrathin c-Si has a high absorption only in a narrow wavelength range around 600 nm, while the Si nanopyramid textured thin films (both periodic and random ones) have excellent light absorption over a broad wavelength. Moreover, the absorption spectrum of the random nanopyramid textured Si is much smoother and higher than that of the periodic one in the long wavelength range, except lower at some peaks. The result explicitly demonstrates the outstanding light trapping effect of random Si nanopyramids in ultrathin c-Si, which is of paramount importance for application. As we know, without additional control (e.g., masking process), the naturally formed Si nanopyramids are randomized, such as our fabricated ones, because of the slight variation of reactants and temperatures as well as the disordered structure nucleus on the surface. The superior light trapping property of the random Si nanopyramids releases the necessary of the masking process to form periodic or ordered Si nanopyramids, and thus the fabrication process is much simpler and cheaper without losing the light absorption.

It is well known that random micropyramids also facilitate the realization of good light trapping in Si wafer by multiple internal reflections.[32] However, when the size of the Si pyramids is comparable to light wavelength, such as our experimentally fabricated and simulated ones, wave optics instead of geometrical optics should be used to explain the light trapping behavior. Here, we investigate the electric-field-intensity distributions in the ultrathin c-Si to reveal the origin of the exceptional light trapping effect of the Si nanopyramid textures, shown in **Figure 8**. At the short wavelength region (451 nm), the electric field in the ultrathin c-Si is rather weak for the planar surface case because most of the light is reflected back into the air by constructive interference from SiN$_x$ layer, whereas in the case of Si nanopyramid textured surface, Si nanopyramids tend to provide Mie resonance scattering, thus leading to the localized resonance of electric field that contributes to the great light absorption enhancement. At the middle wavelength (603 nm), the electric field in the ultrathin c-Si with planar surface is greatly enhanced due to destructive interference and Fabry–Perot resonance. For Si nanopyramidal surfaces, besides Mie resonance and Fabry–Perot resonance, index-guided resonance is also excited by providing phase-matching of incident light to couple to the guided modes.[33] Under this circumstance, all the ultrathin c-Si membranes have ultrahigh light absorption (see Figure 7d). At the long wavelength (1058 nm), due to the deviation of destructive interference, the electric field intensity in the planar ultrathin c-Si is decreased but Fabry–Perot resonance is reserved, thus leading to the decrease of absorption in oscillation. While for the Si nanopyramid textured surface, strong Mie resonance, guided resonance, and Fabry–Perot resonance can still be observed, thereby much higher light absorption than the planar counterpart. Furthermore, we can also observe that the localized resonances in the random nanopyramid textured ultrathin c-Si are distorted as compared to those
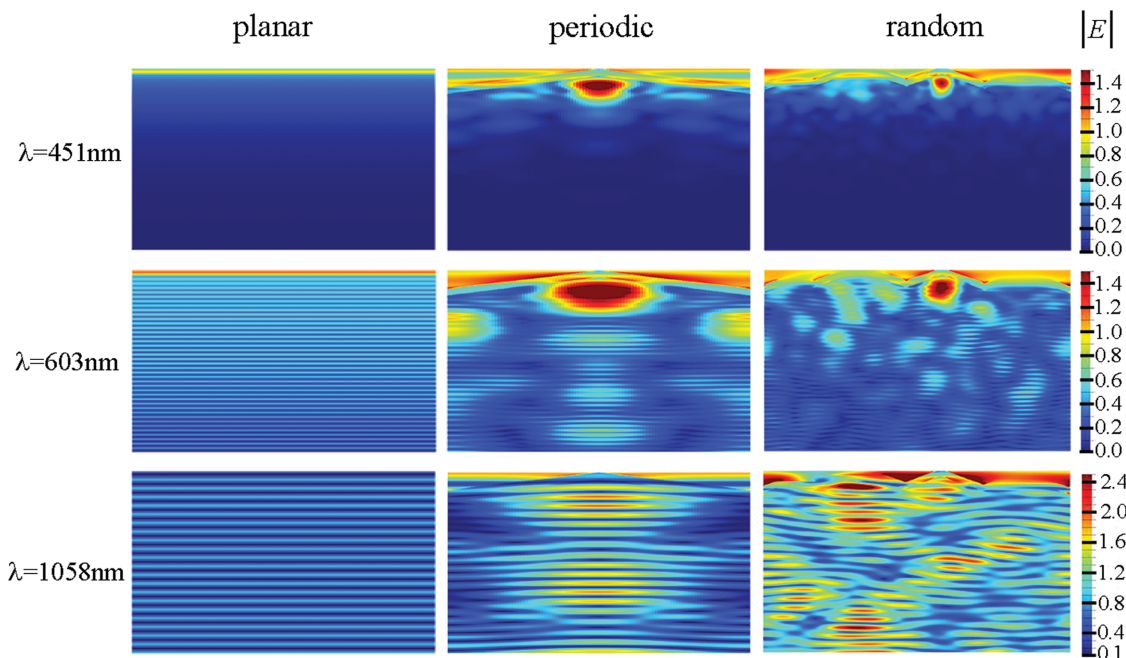
**ADVANCED
FUNCTIONAL
MATERIALS**
www.afm-journal.de

*Materials
Views*
www.MaterialsViews.com

Figure 8. Electric field distributions in the ultrathin c-Si with planar, periodic Si nanopyramid, and random Si nanopyramid textured surface at the incident wavelength of 451, 603, and 1058 nm.

in the periodic counterpart but with a larger and more uniform spatial distribution, which may be attributed to the excitation of more resonant modes. We believe that random Si nanopyramids provide stronger light scattering to induce spectrally broadened resonances.[20,21] Therefore, the random Si nanopyramid textured ultrathin c-Si possesses superior light absorption over the entire spectrum. In fact, in recent years, superior broadband light trapping effect indeed has been demonstrated in disordered nanostructures.[19,20,34] Here, it is worth pointing out that the above optical mechanisms cannot be fully applied to an ultrathin c-Si film with a rather large thickness. For instance, the Fabry–Perot interferences would not take place anymore. Also, the effect of guided resonance weakens or even disappears. And the shorter the wavelength, the weaker the resonance. These phenomena will incur much smoother light absorption spectrum such as the 30-μm-thick case in experiment. However, our simulation results are still meaningful to understand the advantage and light trapping mechanisms of random nanopyramids in ultrathin c-Si film, especially that with the thickness of only several micrometers.

7. Conclusions

The proposed fabrication technique of random Si nanopyramids is all-solution processing, free of electron or ion etching process or dielectric layer as etching mask, and thus is much simpler and more cost-effective. Though Ag nanoparticles play an important role in the formation of Si nanopyramids, the etching mechanism is completely different from that in the acid solution system, where Ag nanoparticles locally accelerate the etching. In our case, the success to form the Si nanopyramids lies in the transfer of the generation position of bubbles from Si surface

to Ag nanoparticles surface so that OH^- ions can react with the entire Si surface to naturally result in random and dense Si pyramid nucleus. Focusing on the application in ultrathin c-Si solar cells, the Si nanopyramids should be fabricated under the solution temperature of 55–65 °C and a short etching time to limit the thickness loss while keep a good antireflection ability. Also, the Ag nanoparticles need to be thoroughly cleaned before the rest of the solar cell is processed in order to avoid destroying the electrical performance. One important character of our fabricated Si nanopyramids is the randomization of both position and size (mainly in the range of 250–650 nm). Excitingly, we find that the random Si nanopyramids facilitate achieving near-Lambertian light trapping in ultrathin c-Si, performing far better than the planar surface and also better than the periodic ones due to more optical resonance modes excited. Therefore, the random Si nanopyramids fabricated by the novel all-solution-processed technique open a new opportunity to enhance the light absorption of ultrathin c-Si solar cells with lower cost.

8. Experimental Section

Sample Fabrication: First, the raw <100> oriented Si wafers (p-type with resistivity of 1–3 Ω cm and thickness of 190 μm) were cleaned in acetone solution with ultrasonic stirring for 40 min, and then etched in NaOH solution with a concentration of 10% at a temperature of 80 °C for 90 s to remove the saw-damage layer and form polished surface. After that, these wafers were immersed in a mixed solution of 7.8×10^{-3} M AgNO$_3$ and 9.6 vol% HF for 10 s at room temperature to form an Ag nanoparticle layer. Subsequent anisotropic etching in a mixed solution of 1.1% NaOH and 8 vol% IPA was carried out to produce Si nanopyramids, followed by removing the Ag nanoparticles in HNO$_3$ solution and removing silicon oxide layer in HF solution. Note that, the Si wafers need to be immersed in deionized water between every two steps mentioned above to remove

the residual etching solution. Si micropyramids were also fabricated as the counterparts by anisotropic etching (1.2% NaOH and 8 vol% IPA) for 40 min under the solution temperature of 80 °C.

The ultrathin c-Si samples were obtained by etching the bulk p-type c-Si wafer with resistivity of 1–3 Ω cm and thickness of 190 μm for 80 min in 10% NaOH solution under the temperature of 80 °C. The resultant thin film layer has a thickness of 30 μm. After Si nanopyramids were fabricated on the ultrathin c-Si surfaces, SiN$_x$ layers were deposited on both surfaces with plasma enhanced chemical vapor deposition (the thicknesses for the front side and back side were different and controlled by the deposition time), and then Ag films were deposited onto the back SiN$_x$ layer as back reflector by electron beam evaporation.

FDTD Simulation: In the simulation, to explore the advantage of random Si nanopyramids on ultrathin c-Si film and reveal the light trapping mechanism, a substrate thickness of 3 μm was employed and periodic Si nanopyramids as well as planar surface were simulated for comparison. In the periodic case, the size of pyramids and the period are 500 nm (*xy*-plane). In the random case, 16 Si nanopyramids with sizes ranging from 300 to 700 nm were randomly distributed in a 1500 × 1500 nm square with periodic boundary conditions (*xy*-plane). Some pyramids were partly overlapped, which is consistent with the experimental fact. The results of four distinct random configurations were averaged as the properties of random arrays. The ratio of the height to the bottom length of the Si pyramids was fixed to be 1.37 (corresponding to that the angle between the slope facet and the bottom facet was 54°). All the surfaces (periodic, random, and planar) were covered by SiN$_x$ layer with a thickness of 75 nm. Ag layer (200 nm) and SiN$_x$ layer (100 nm) were coated at the rear side of the ultrathin c-Si, as shown in Figure 7. The light source was plane wave directed to the minus *z*-axis (which is normal incidence for the planar surface) with wavelength ranging from 300 to 1100 nm. The top boundary of the *z*-axis direction is perfectly matched layer, while the bottom boundary is metal layer. A power monitor was positioned above the light source to obtain the *R* and an absorption monitor was used to obtain the light absorption in the Ag layer (A_{Ag}), so the absorption in ultrathin c-Si was calculated by $1 - R - A_{Ag}$. Another power monitor located in the *y*-normal plane was used to obtain the distribution of electric field intensity in the ultrathin c-Si. All the above simulations were performed using a commercial software package (FDTD Solutions v8, Lumerical 2013), from which the optical constants of Si were directly extracted. The refractive indexes of SiN$_x$ were set to be a constant value of 2 without considering the extinction coefficient.

Characterization: The micromorphologies of the Si surface were investigated by field emission scanning electron microscopy. The mass of the Si was weighted by electronic balance with accuracy of 0.0002 g. The polished wafer thickness was measured by optical microscope. Image Tool as well as Nano Measurer software were employed to calculate the size and coverage of Si pyramids. The *R* and transmittance (T_{ran}) of the ultrathin c-Si were measured by UV–vis–NIR spectroscopy with integrating sphere, and thus the A_b in the ultrathin c-Si can be calculated to be $1 - R - T_{ran}$.

Acknowledgements

[1] S. Jeong, M. D. McGehee, Y. Cui, *Nat. Commun.* **2013**, *4*, 2950.
[2] A. Rahman, A. Ashraf, H. Xin, X. Tong, P. Sutter, M. D. Eisaman, C. T. Black, *Nat. Commun.* **2015**, *6*, 5963.
[3] T. J. Kempa, R. W. Day, S.-K. Kim, H.-G. Park, C. M. Lieber, *Energy Environ. Sci.* **2013**, *6*, 719.
[4] S. E. Han, G. Chen, *Nano Lett.* **2010**, *10*, 4692.
[5] G. Li, H. Li, J. Y. L. Ho, M. Wong, H. S. Kwok, *Nano Lett.* **2014**, *14*, 2563.
[6] M. S. Branham, W.-C. Hsu, S. Yerci, J. Loomis, S. V. Boriskina, B. R. Hoard, S. E. Han, G. Chen, *Adv. Mater.* **2015**, *27*, 2182.
[7] A. Mavrokefalos, S. E. Han, S. Yerci, M. S. Branham, G. Chen, *Nano Lett.* **2012**, *12*, 2792.
[8] S. Zhong, Z. Huang, X. Lin, Y. Zeng, Y. Ma, W. Shen, *Adv. Mater.* **2015**, *27*, 555.
[9] B.-R. Huang, Y.-K. Yang, W.-L. Yang, *Appl. Surf. Sci.* **2013**, *266*, 245.
[10] J. Kim, D. Inns, K. Fogel, D. K. Sadana, *Sol. Energy Mater. Sol. Cells* **2010**, *94*, 2091.
[11] C. Liu, *J. Korean Phys. Soc.* **2014**, *64*, 1239.
[12] G. Li, Y. Zhou, F. Liu, *J. Non-Cryst. Solids* **2012**, *358*, 2223.
[13] Y. Wang, L. Yang, Y. Liu, Z. Mei, W. Chen, J. Li, H. Liang, A. Kuznetsov, X. Du, *Sci. Rep.* **2015**, *5*, 10843.
[14] J. Kim, U. Plachetka, C. Moormann, H. Kurz, *Microelectron. Eng.* **2013**, *110*, 403.
[15] J.-Y. Chen, M.-H. Yu, S.-F. Chang, K. W. Sun, *Appl. Phys. Lett.* **2013**, *103*, 133901.
[16] M. Koh, S. Sawara, T. Shinada, T. Goto, Y. Ando, I. Ohdomari, *Appl. Surf. Sci.* **2000**, *162*, 599.
[17] Z. Yu, A. Raman, S. Fan, *Opt. Express* **2010**, *18*, A366.
[18] X. Fang, M. Lou, H. Bao, C. Zhao, *J. Quant. Spectrosc. Radiat. Transfer* **2015**, *158*, 145.
[19] K. Vynck, M. Burresi, F. Riboli, D. S. Wiersma, *Nat. Mater.* **2012**, *11*, 1017.
[20] B. C. P. Sturmberg, K. B. Dossou, L. C. Botten, A. A. Asatryan, C. G. Poulton, R. C. McPhedran, C. M. de Sterke, *Appl. Phys. Lett.* **2012**, *101*, 173902.
[21] U. W. Paetzold, M. Smeets, M. Meier, K. Bittkau, T. Merdzhanova, V. Smirnov, D. Michaelis, C. Waechter, R. Carius, U. Rau, *Appl. Phys. Lett.* **2014**, *104*, 131102.
[22] M. A. Green, *Prog. Photovoltaics Res. Appl.* **2002**, *10*, 235.
[23] E. Yablonovitch, *J. Opt. Soc. Am.* **1982**, *72*, 899.
[24] E. Vazsonyi, K. De Clercq, R. Einhaus, E. Van Kerschaver, K. Said, J. Poortmans, J. Szlufcik, J. Nijs, *Sol. Energy Mater. Sol. Cells* **1999**, *57*, 179.
[25] C. Chartier, S. Bastide, C. Lévy-Clément, *Electrochim. Acta* **2008**, *53*, 5509.
[26] C.-Y. Chen, C.-P. Wong, *Nanoscale* **2015**, *7*, 1216.
[27] H. Seidel, L. Csepregi, A. Heuberger, H. Baumgärtel, *J. Electrochem. Soc.* **1990**, *137*, 3612.
[28] K. Peng, H. Fang, J. Hu, Y. Wu, J. Zhu, Y. Yan, S. Lee, *Chem. Eur. J.* **2006**, *12*, 7942.
[29] Z. Huang, N. Geyer, P. Werner, J. De Boor, U. Gösele, *Adv. Mater.* **2011**, *23*, 285.
[30] K. B. Sundaram, A. Vijayakumar, G. Subramanian, *Microelectron. Eng.* **2005**, *77*, 230.
[31] Z. C. Holman, S. De Wolf, C. Ballif, *Light: Sci. Appl.* **2013**, *2*, e106.
[32] P. Campbell, M. A. Green, *J. Appl. Phys.* **1987**, *62*, 243.
[33] M. L. Brongersma, Y. Cui, S. Fan, *Nat. Mater.* **2014**, *13*, 451.
[34] A. Bozzola, M. Liscidini, L. C. Andreani, *Prog. Photovoltaics Res. Appl.* **2014**, *22*, 1237.